Ocean Engineering 220 (2021) 108435

Contents lists available at ScienceDirect

Ocean Engineering

journal homepage: www.elsevier.com/locate/oceaneng

Moving source identification in an uncertain marine flow: Mediterranean Sea application

Mohamad Abed El Rahman Hammoud [a], Issam Lakkis [b], Omar Knio [a], Ibrahim Hoteit [a,*]

[a] King Abdullah University of Science and Technology, Thuwal, 23955, Saudi Arabia
[b] Department of Mechanical Engineering, American University of Beirut, Beirut, Lebanon

ARTICLE INFO

Keywords:
Marine pollution
Source identification
Lagrangian tracking
Moving source
Stochastic flow field

ABSTRACT

Identifying marine pollutant sources is essential to assess, contain and minimize their risk. We propose a Lagrangian Particle Tracking algorithm (LPT) to study the transport of passive tracers advected by an uncertain flow field described by an ensemble of realizations of the ocean currents, and to identify the source parameters of the release in backward mode. Starting from a probability map describing the distribution of a pollutant, reverse tracking is used to generate probabilistic inverse maps by integrating it with the ensemble of flow fields backward in time. An objective function based on the probability-weighted distance between the resulting inverse maps and the source trajectory is then minimized to identify the likely source of pollution. We conduct numerical experiments to demonstrate the efficiency of the proposed algorithm in the Mediterranean Sea. Passive tracers are released along the path of a ship and propagated with an ensemble of realistic flow fields to generate a probability map, which is then used for the inverse problem of source identification. Our results suggest that the proposed algorithm captures the release time and source of pollution, successfully pinpointing to the release parameters up to two weeks back in time in certain case studies.

1. Introduction

Modeling the transport of species and pollutants in the ocean is important for a variety of applications, including search and rescue (Otote et al., 2019), risk assessment (Niu et al., 2010; Havens et al., 2010), and ecosystem management (Raitsos et al., 2017; Wang et al., 2019). This is often used to determine the trajectory and final destination of pollutants. Particle tracking of pollutants in water bodies has been extensively studied for a deterministic flow (e.g. Kao and Elsayed (1990)), and also for an uncertain (stochastic) flow (e.g. Zhao et al. (2011); El-Mohtar et al. (2018)). In a stochastic framework, the solution of the particle tracking problem is described by a probability map that indicates the likelihood of a particle reaching a certain location (Beaudoin et al., 2007; El-Mohtar et al., 2018).

Lagrangian Particle Tracking (LPT) algorithms, which track individual particles in a Lagrangian framework, are commonly used to model the transport of matter in a flow field (Kao and Elsayed, 1990; Brickman and Smith, 2002; Batchelder, 2006). Such algorithms can be coupled with physical models to study the transport of specific types of particles. For instance, the LPT can be coupled with certain biological modules to investigate the transport of nutrients and fish larvae in water bodies (Petihakis et al., 2002; Sentchev and Korotenko, 2007; Lett et al., 2008). Another use of this algorithm is to track micro-plastics and study their spread (Wichmann et al., 2019). LPT was also used for simulating oil spills (De Dominicis et al., 2013b), such as the Deepwater Horizon in the Gulf of Mexico (North et al., 2013; Liu et al., 2013), after augmenting it with diffusion and oil weathering to describe the coupling between physical and chemical processes such as emulsification, evaporation and dispersion (North et al., 2013; Liu et al., 2013). A thorough review of recent advances in ocean applications of Lagrangian tracking algorithms can be found in van Sebille et al. (2018). The use of LPT also extends to the field of medicine and drug delivery, where models for micro-scale motion are implemented to track the transport of drugs in the human body (Pourmehran et al., 2015; Schuster et al., 2015).

Uncertainties in particle tracking are associated with uncertainties in processes particles undergo and in the oceanic flow field, which arises from the imperfect representation of the ocean forcing, initial conditions, and internal physics (Groves et al., 2008; Bennett et al., 2012; Edwards et al., 2015; Hoteit et al., 2018). Uncertainties in the oceanic flow are commonly tackled by advecting particles with a stochastic flow field represented by an ensemble of realizations (Beaudoin et al., 2007; Guo et al., 2013, 2019; El-Mohtar et al., 2018). In this sense, at each time

* Corresponding author.
E-mail address: ibrahim.hoteit@kaust.edu.sa (I. Hoteit).

https://doi.org/10.1016/j.oceaneng.2020.108435
Received 20 April 2020; Received in revised form 14 October 2020; Accepted 29 November 2020
Available online 9 December 2020

step, the velocity field consists of a set of realizations representing possible scenarios of the ocean currents (Hoteit et al., 2013). Recently, El-Mohtar et al. (2018) investigated an LPT algorithm operating with an ensemble of flow fields of the Red Sea. This algorithm advects particles in a parallel framework and introduces a cost-effective binning scheme that groups spatially close particles in order to cap the number of particles to avoid memory and storage issues. Similarly, Guo et al. (2013) investigated the advection of particles in a stochastic atmospheric flow, and constructed a variational field, which characterizes the differences in ensemble runs based on the different pathlines obtained for each particle.

The Mediterranean Sea is a busy waterway responsible for around 15% of the global shipping activity (Kostianoy and Carpenter, 2018a), offering a passageway for different types of ships: recreational, shipping, tankers, etc. (Girin and Carpenter, 2018), and hosting many oil platforms along its coast (Kostianoy and Carpenter, 2018b). It is therefore prone to marine pollution from fixed platforms and from moving ships. According to Kostianoy and Carpenter (2018b), 14 accidental oil spills occurred in the Mediterranean between 1970 and early 2016 that contaminated the sea with more than 10 tons of oil. The Lebanese oil leak of 2006 is considered as the biggest oil pollution incident in the Eastern Mediterranean (Coppini et al., 2011). LPT models have been extensively applied to the Mediterranean Sea to study various transport phenomena, such as micro-plastics (van Sebille et al., 2015; Liubartseva et al., 2016, 2018; Duncan et al., 2018), and oil. Some of the well-developed oil spill models are Poseidon (Annika et al., 2001; Perivoliotis et al., 2011), MEDSLIK (Zodiatis et al., 2012, 2017; Lardner and Zodiatis, 2016, 2017) and MEDSLIK II (De Dominicis et al., 2013a, b).

LPT algorithms can also be operated in reverse mode to investigate the inverse problem of source identification, which only requires direct integration of the particles backward in time when time-reversible terms are involved (Brickman and Smith, 2002; Batchelder, 2006; Breivik et al., 2011). This generally becomes noticeably more complex for nonlinear irreversible problems, which may require more advanced inverse approaches, such as Bayesian inference (Yee, 2007), or more sophisticated integration techniques such as operator splitting (Ivorra et al., 2016). Until recently, source identification in ocean studies has been restricted to a single source applications with a deterministic flow field. Zodiatis et al. (2012) tackled the problem of determining multiple sources in a deterministic flow by integrating contours and particles backward in time. El-Mohtar et al. (2018) addressed the problem of source identification of a single release source in a probabilistic framework by integrating a single particle backward in time using an ensemble of flow fields and generating a spatial distribution describing the likelihood of where the particle might be located.

In this work, we first investigate the transport of particles from fixed and moving sources with an uncertain flow. We then introduce and test a new approach to identify the contamination source based on an objective function described by the distance between the inverse probability maps and the paths of different ships, weighted by the probability associated with individual particle locations found by inverse tracking. The proposed methodology is computationally very efficient and can be utilized with any LPT algorithm capable of backward integration (Brickman and Smith, 2002; Batchelder, 2006; Breivik et al., 2011; Zodiatis et al., 2012; De Dominicis et al., 2013a, b; El-Mohtar et al., 2018). This could also be particularly useful to provide timely support for a first fast response of a spill, for instance, in an operational setting when the composition of the pollutant is not known, or when weathering processes cannot be accurately modeled. We demonstrate the efficiency of the proposed framework by conducting realistic numerical experiments to identify the source of pollution in the Mediterranean Sea advected by an uncertain flow. The experiments indicate that under certain conditions that do not include heavy beaching effects, the release source and time of pollutants may be efficiently predicted up to two weeks after the release. The sensitivity of the objective function to the observation time and flow variability is also examined.

The paper is structured as follows. The LPT methodology is described in Section 2, with a focus on continuous particle release from both fixed and moving sources in an uncertain flow field. Section 3 presents the proposed algorithm for source identification. The design of the numerical experiments is outlined in Section 4, and the results are analyzed and discussed in Section 5. Conclusions and final remarks are offered in Section 6.

2. Forward tracking

We build on the LPT algorithm presented by El-Mohtar et al. (2018) to advect particles released from a single source at a given time with deterministic and stochastic flow fields. The algorithm efficiently deals with particle advection through parallelization, and controls the growth of the number of particles when advected with an ensemble of flow fields by binning. Integration for particles location is carried out using a 4^{th} order Runge Kutta scheme to solve for the unsteady advection equation governing the transport of passive particles at each integration (advection) time step, δt. In an uncertain setting, the released particle is advected by each of the realizations of the ensemble of flow fields, with each realization representing a possible scenario for the transport of a particle at that specific location. This generates a spatial distribution of the particles with associated probabilities of being at the corresponding location; this distribution is referred to as a probability map. To overcome computational issues arising from the exponentially growing number of particles, particles are binned so that the total number of particles is capped to a maximum (Hollt et al., 2015). Bins are defined as refined spatial cells, where particles belonging to the same bin are grouped into a single particle. Here, binning is spatially adaptive with smaller bins assigned to regions of higher probability and smaller variance; the smallest bin has quarter the dimension of the computational grid cell in each direction. Binning is also designed to conserve the first two moments of probability of the particles to be at a given location before generating new particles with new weights, where the weight of a particle is defined as the scaled probability of a particle being at a given location (El-Mohtar et al., 2018).

A new particle injection mode is developed here to allow for a continuous release of particles from fixed and moving sources. This model is schematized in Fig. 1 where new particles are released at each advection time step and advected from the release time till the end of the simulation time. This staged injection-advection allows to keep track of the time stamp of particles, mimicking a realistic release. Fractional time stamping associated with the newly injected particles is used in the staged release to ensure their release at the intended time. The time fraction is the ratio of the time elapsed from the current LPT model time

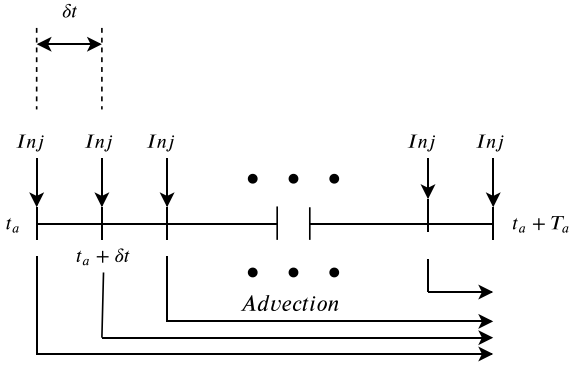

Fig. 1. Continuous release modeled based on the staged release of particles. The particles are advected from the individual time of release till the end of the simulation time. Within a period T_a, we inject $\frac{T_a}{\delta t}$ particles at uniform increments of size.δt

step to the time between two consecutive velocity fields.

Particles can be released from a fixed location, denoted by $\vec{x}_{inj}$, at every advection time step. Particles can also be continuously released from a moving source of fixed path and speed. The injection locations are determined based on the velocity and initial location of the moving source, which can be expressed as:

$$\vec{x}_{inj} = \vec{u}_{src} \cdot t_{inj} + \vec{x}_0, \tag{1}$$

where t_{inj} is the injection time. The release can last for as long as the ship is moving along the path, where particles are released in stages and advected till the end of the simulation time. Based on the staged injection, a particle is released at the chosen location of the moving source at the exact time it crosses this location. For an ensemble of flow fields, every particle is then advected by each realization of the currents where particles that end up in the same bin are grouped into a single bin while conserving the first two moments of probability as performed by El-Mohtar et al. (2018).

3. Inverse tracking and source identification

The inverse problem of identifying the source of a pollution patch released from a moving source starts with a standard LPT framework operating in reverse (De Dominicis et al., 2013a; El-Mohtar et al., 2018). Starting from an observed distribution of particles, which may be deterministic or probabilistic, particles are first sampled from this distribution before they are advected back to a selected time with the reversed currents. An initial probabilistic distribution of this inverse problem may for instance represent an uncertain spatial map of particles locations inferred from a satellite image, where such uncertainties may arise from imperfections in remote sensing and processing, such as pixel noise and error bars in the classification algorithm (Wang et al., 2009; Zhang and Zhang, 2019). Since the actual release time of the particles could also be an unknown, inverse time integration is performed till a selected time prior to the release, which is believed to be close to the release window, where the release window is defined as the time frame between the start and end time of the release.

Upon integrating the observed distribution backward in time, a new inverse probability map is generated at every integration time step. The inverse probability map represents the uncertainty in the particles location, generated based on the particle distribution at every inverse time step. An objective function is formulated based on the geographical distance between the inverse probability map and the moving source trajectory. The objective function is designed so that its minimum occurs at the release time where the inverse probability map and the release segment are spatially closest to each other. To identify a pollution source, this objective function is computed for different ship trajectories in the area near the spill. The minima are compared to identify the most probable culprit, which corresponds to the smallest objective function.

Different forms of such an objective function were investigated, including the shortest and average distances. The objective functions are normalized for a more straightforward comparison between the distances associated with the particle distributions obtained from deterministic and stochastic flows. The first objective function measures the shortest distance between the points of the discretized probability map and the trajectory, scaled by the probability of a particle lying in the cell and normalized by the total sum of probabilities of the particles to be at their corresponding locations. Such distances are schematized in Fig. 2, which shows the projections from some points of the probability map to the release path. The distances are summed over all the points of the inverse probability map to produce the objective function based on the shortest distance, which is expressed as:

$$J^k_{shortest} = \sum_{i=1}^{N_{pts,map}} \frac{p_i}{\sum_{j=1}^{N_{pts,map}} p_j} ||\boldsymbol{x}_i - \boldsymbol{x}^k_{p,i}||, \tag{2}$$

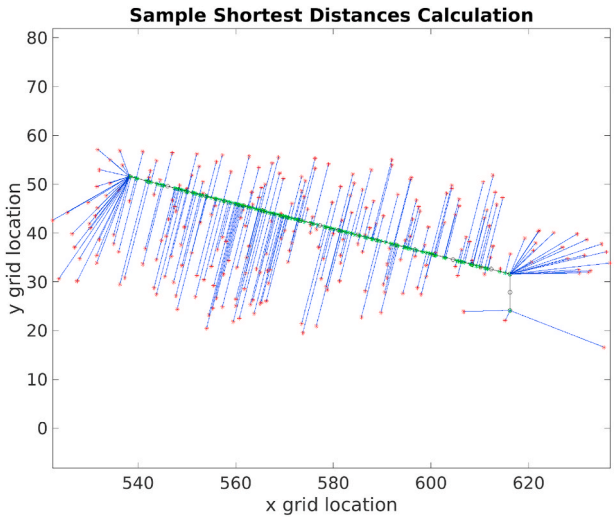

Fig. 2. Schematic of the projections between selected points of the probability grid and the trajectory. Red stars are some chosen points of the probability map, black circles are the points forming the path, green points are the projection of the red stars onto the path, and the blue line represents the shortest distance. (For interpretation of the references to color in this figure legend, the reader is referred to the Web version of this article.)

where J^k is the objective function corresponding to the k^{th} trajectory, $\boldsymbol{x}_i$ is the position of the point on the grid cell, $\boldsymbol{x}^k_{p,i}$ is the position of the projection of $\boldsymbol{x}_i$ on the k^{th} trajectory, p_i is the likelihood at the i^{th} point of the probability map and $N_{pts,map}$ is the number of particles forming the probability map. The objective function based on the average distance is evaluated as the sum of the distances between the inverse probability map and each of the points forming the trajectory, scaled by the probability of the particle being there. This can be expressed as:

$$J^k_{average} = \sum_{i=1}^{N_{pts,map}} \sum_{j=1}^{N_{pts,traj.}} \frac{p_i}{N_{pts,traj.} \sum_{j=1}^{N_{pts,map}} p^k_j} ||\boldsymbol{x}_i - \boldsymbol{z}^k_j||, \tag{3}$$

where $\boldsymbol{z}^k_j$ represents the points forming the k^{th} trajectory, and $N_{pts,traj.}$ corresponds to the number of points forming the trajectory. In our linear model, the objective function, in its two forms, is convex having a minimum at the expected release time.

In order to determine the release location and time using a given observation, a number of candidate trajectories of moving sources that have recently passed near the study region are first identified. After computing the objective function and comparing the resulting distances, some trajectories can be discarded since they are farther from the probability map than other trajectories. In most situations, a few close trajectories can be selected as possible candidates. This can be addressed by tracking the time when ships passed through the release location using Automatic Identification Systems (e.g. MarineTraffic – Global Ship Tracking Intelligence www.marinetraffic.com).

To illustrate the form of the objective functions, an experiment is conducted in which particles were released at hourly increments along a ship path extending from 35°N, 22°E to 36°N, 16°E over a period of one day, from Day 3 till Day 4 of the simulation time. Fig. 3 plots sample results for the proposed objective functions, showing convex shapes for both objective functions. For the test shown, the two objective functions defined in Equations (2) and (3) point to different minima, with the shortest distance-based objective function being able to accurately pinpoint the release time as opposed to the average distance-based approach which was 3 days off, as can be seen in Fig. 3. In particular, in the case of a continuous release, the proposed methodology would point to the end of the release window, after all the particles are released into the ocean. This was observed in our study where the data is

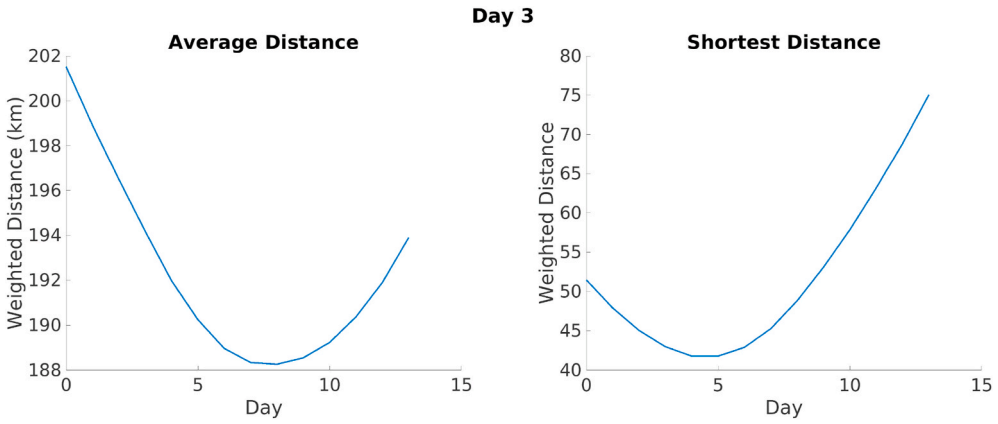

Fig. 3. Plots portraying different methods for computing the weighted distances. The distances are computed between inverse probability maps of a release that started at Day 3, and the release segment. The case study starts from an observation at Day 15 and goes back to Day 1. The distance at Day 15 is not shown as the observation can not match the release.

available at a daily rate. After extensive testing, the shortest distance formulation was selected as the better approach.

4. Experiments design

4.1. Experimental setup

Experiments are conducted to assess the performance of the proposed algorithm. To test the continuous release of particles from a fixed source, we place the source location at the South of the Ionian Sea at 18°E 34.6°N and continuously release particles at an hourly rate for a period of one day.

For the moving source experiment, we opted to use a ship trajectory that is densely operated by vessels. We first examined the vessel routes' density in order to choose a route that is representative of a real case scenario. The density map for the vessels in the Mediterranean is shown in Fig. 4, which outlines how congested the Mediterranean is in terms of annual number of ships. From the density map, a path of high density is selected. The chosen path is for a ship traversing the Mediterranean Sea westwards starting from the Suez Canal and leaving through the Strait of Gibraltar. Release segments were chosen to represent single day releases based on a ship that moves at a constant speed. The chosen path is split into seven segments, each segment corresponding to continuous ship motion over a single day, traveling at a constant speed of 14 knots, corresponding to a typical tanker or bulk carrier. These release segments are illustrated in Fig. 5. A single-day release period was chosen to mimic an emergency scenario, an example of such is the Lebanon Jiyyeh oil spill which lasted for approximately 2 days (Coppini et al., 2011). The experiments focus on the Day 3 release path with a release window between Days 3 and 4, with the exception of Section 5.4 in which we study the release from the Day 1 path due to the heavy beaching observed in its vicinity.

Simulations are conducted using the ensemble of velocity fields described in Section 4.2, advecting particles every hour. As for the inverse simulation, particles were integrated two week back to reach the first data time step, which was Day 0 in our experiments. Finally, we use a maximum of 100 million particles for all simulations following the results of El-Mohtar et al. (2018), who suggested that a maximum number of particles greater than 50 million is needed to capture the details of the particle distribution.

4.2. Generating a flow field ensemble

Copernicus Marine Environment Monitoring System (CMEMS) offers

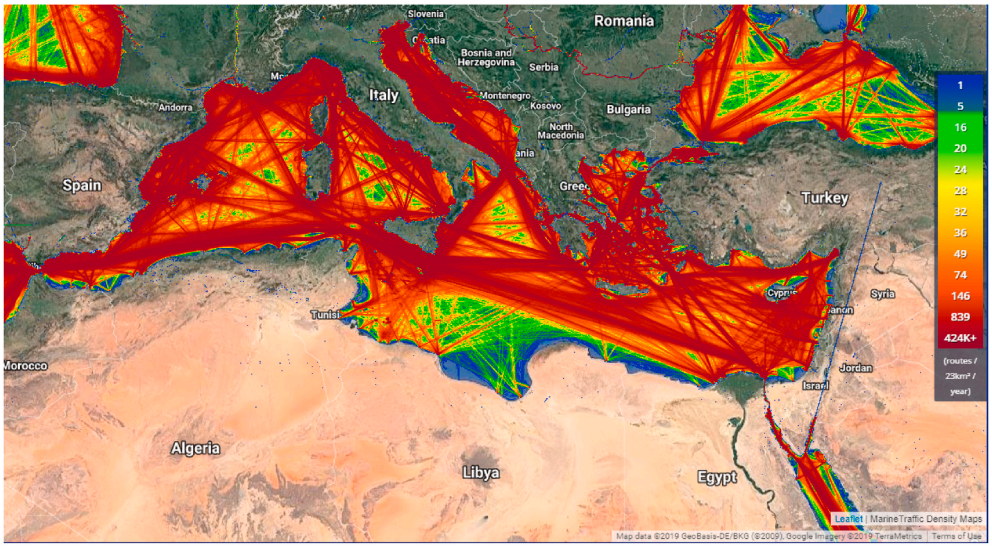

Fig. 4. Contours depicting the marine traffic density in the Mediterranean. The density is defined for the number as ships per 23 km^2 averaged over a year (see https://www.marinetraffic.com).

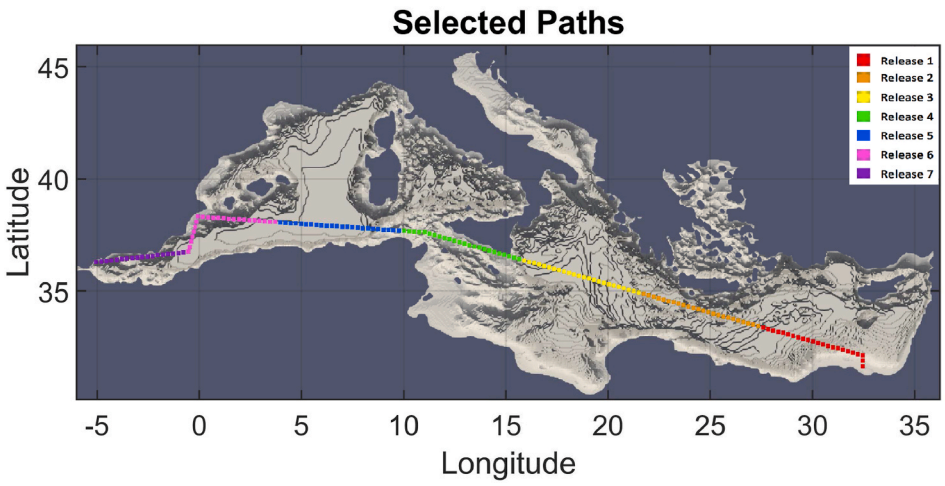

Fig. 5. Individual paths (colors) selected for case study. One of the highest density paths is chosen and divided into seven individual segments. (For interpretation of the references to color in this figure legend, the reader is referred to the Web version of this article.)

30 years of reanalysis fields for the Mediterranean Sea, based on which we generate an ensemble of realizations of the ocean currents to mimic a probabilistic framework. The reanalysis spans the Mediterranean from -6.00° to 36.25° in longitude, 30.17° to 45.9375° in latitude, and a depth stretching down to $5334.65m$ below sea level. The data is uniformly spaced horizontally with a resolution of $0.0625^\circ \times 0.0625^\circ$, and non-uniformly spaced in depth with 72 levels; corresponding to $677 \times 253 \times 72$ grid points. The reanalysis is available over a 30 years period from 1987 till 2016, from which we focus on the time frame between the 14^{th} of July and the 12^{th} of August. This provides a sufficient time span to examine long time integration and discontinuous releases. The whole reanalysis dataset was also used for generating an ensemble of flow fields as described below.

An ensemble of realizations of the sea currents is randomly generated for each day of the simulation period based on a normal distribution with mean as the background velocity and covariance as that of the reanalysis velocity fields on that same day of each year, for a total of 30 fields. In order to include more realizations for a given date, windows of ± 0, 1 and 2 days about the day of interest were examined, based on which, a window of ± 1 day was found sufficient to sample smooth fields. An Empirical Orthogonal Function (EOF) Analysis is then performed to filter out low time-variance features, generally of small scales nature in the ocean, before sampling (Golub and Reinsch, 1971; Preisendorfer and Mobley, 1988; Hoteit et al., 2001). This is achieved by computing the eigenvectors and corresponding eigenvalues (λ_i^j) of the covariance matrix, C_{d_i}. The eigendirections corresponding to small eigenvalues of the covariance are then truncated to obtain a low-rank approximation, $\tilde{C}_{d_i}$, of C_{d_i}. Here, we select the first eigenvectors that describe at least 95% of the variance of the realizations, according to:

$$\frac{\sum_{j=1}^{r}\lambda_j}{\sum_{j=1}^{M}\lambda_j} > 0.95, \tag{4}$$

where M is the total number of eigendirections and r is the number of retained eigendirections. This low-rank approximation of the covariance is readily decomposed into $\tilde{C} = \tilde{L}\tilde{L}^T$, which is used to generate the members of the ensemble of flow fields as follows:

$$x^i_{dayj} = x_{day_j,2006} + \tilde{L}\gamma^i_{day_j}, \quad \gamma^i_{day_j} \tilde{} \mathcal{N}(0, I_{M\times M}), \tag{5}$$

where, x denotes the longitudinal or latitudinal currents, j is the day of interest, $i = 1, 2...N_e$, and N_e the ensemble size, chosen to be 50 in our experiments, as typically provided by marine weather services. The γ^is are resampled every time step from a normal distribution of zero mean and identity covariance.

The background surface velocity field, the variance of this ensemble, and a few realizations of the surface currents for Day 15 are presented in Fig. 6, suggesting high uncertainty near oceanic mesoscale features such as straits and eddy peripheries, as typically obtained from ocean ensemble data assimilation systems (Hoteit et al., 2010).

4.3. Inverse maps and post-processing

The probability maps are generated at each time step by processing particle distributions using a Gaussian basis function that maps the particle weights into probabilities defined on grid cells (El-Mohtar et al., 2018). It is generally beneficial to post-process the probability maps in order to remove particles with negligible weights and to filter out particles trapped along the coast, where trapped particles are particles that are advected by multiple realizations of small velocity. Particles with negligible weights are usually found along the edge of the slick, and although they have low probabilities, however, since they are far from the ship trajectory they contribute to the objective function causing a deviation of its minimum. Removing particles trapped near the coast, however, is generally useful because these particles were found trapped along the coast by several realizations of small velocities that prevented them from being released back into the ocean, which in turn leads to deviating the minimum of the objective function away from the actual release time.

One straightforward way to filter the particles distribution is to discard unlikely particles whose weights are less than a prescribed threshold. Another way is to evaluate the CDF of the probability distribution, then truncate all the particles in the lower 5% density, which would remove all particles with low probability relative to the whole distribution. It is also possible to truncate all the particles in both the lower and upper 5% of the CDF. This discards all particles with low probabilities, and by removing the top 5% particles, highly concentrated particles near the beach are discarded. This would however remove particles near the trajectory with high probabilities. One may also only disregard particles located in coastal cells, where coastal cells are defined as those with at least one node of the $3D$ grid cell on land. A stricter procedure to handle concentrations of particles near the shore is to remove both coastal and directly neighboring cells. This allows to mitigate beaching effects, where beached particles trapped near the beach would be excluded from calculating distances. Filtering based on coastal cells schemes is illustrated in Fig. 7.

After testing the aforementioned techniques, removing the coastal cells was chosen for filtering the particles distributions for our study. Further discussion is presented in the supplementary material in which

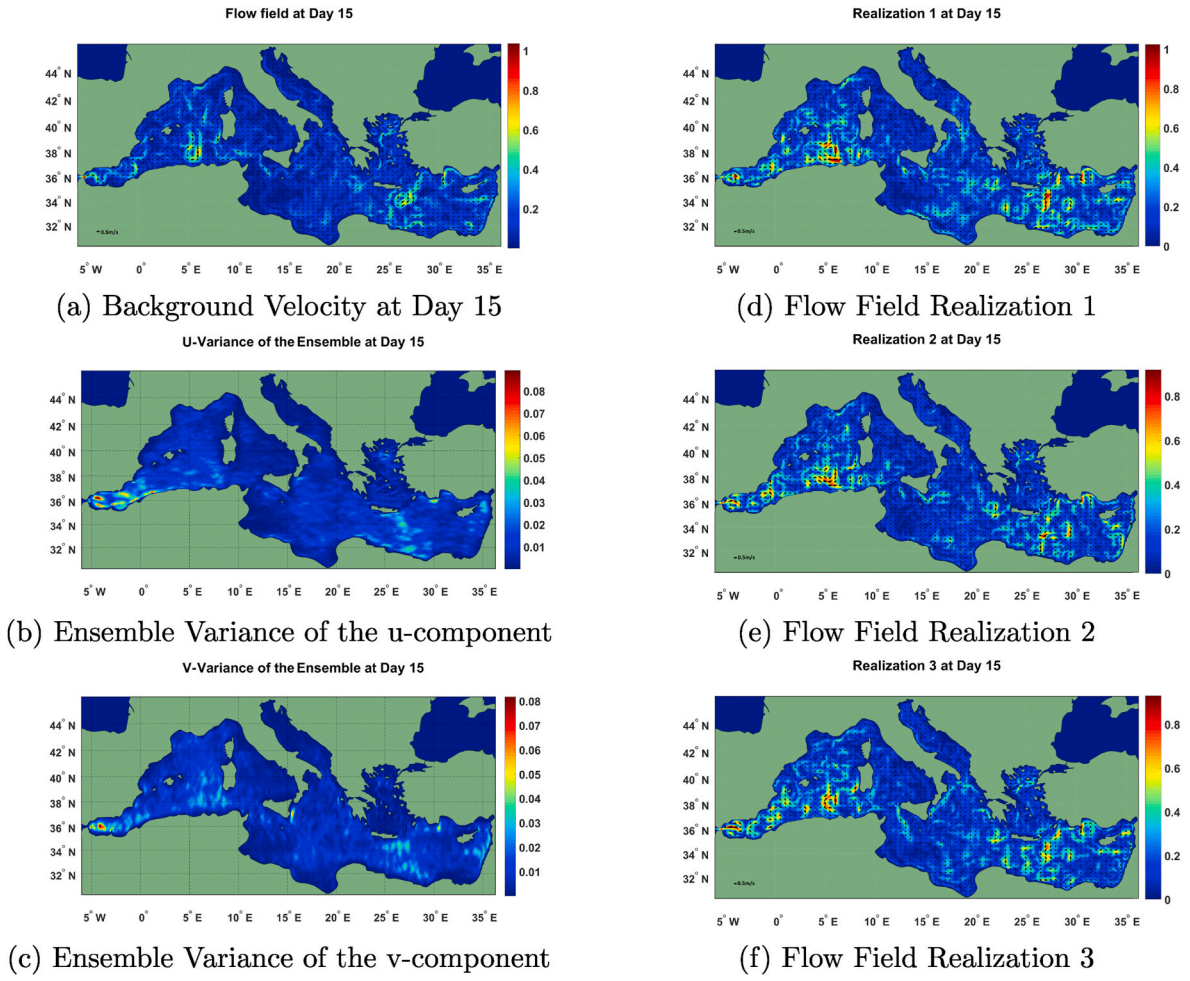

Fig. 6. a) Colormap indicating the velocity field from Copernicus Marine Environment Monitoring Service at Day 15 in (m/s), b) the seasonal variance of the u-component of the velocity at Day 15 in (m^2/s^2), c) the seasonal variance of the v-component of the velocity at Day 15 (m^2/s^2), d) Realization 1 of the sea currents at Day 15 in (m/s), e) Realization 2 of the sea currents at Day 15 in (m/s), f) Realization 3 of the sea currents at Day 15 in (m/s).

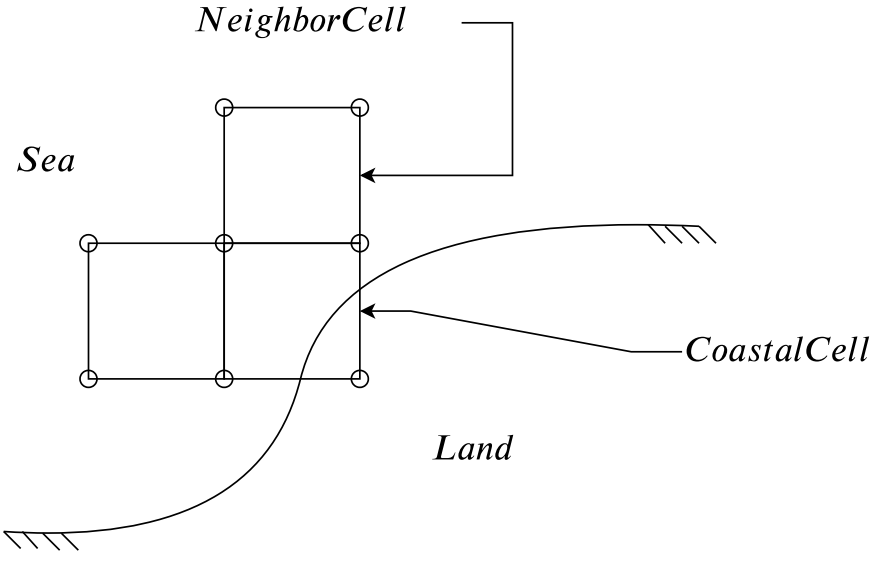

Fig. 7. Schematic defining the coastal cells and neighboring cells. This is the model used for post-processing the particles to compute the distances.

comparisons of the resulting probability maps and distances are discussed.

5. Results

This section presents and discusses the results of the numerical experiments illustrating the implementation of the proposed source identification algorithm for continuous release from fixed and moving sources. In addition, we assess the sensitivity of the algorithm to various parameters, including the size of the observed area, the observation time, and the variance of the ocean currents ensemble.

5.1. Continuous release from a fixed source

In this experiment, particles are released from a source located at 18°E 34.6°N, over a single day, between Days 3 and 4 and advected till Day 30. The resulting probability map at Day 14 is then saved, from which particles for the inverse study are sampled and propagated backward in time. The objective function is then computed at every inverse time step and the minimum is located. These results are presented in Fig. 8.

The forward probability map shows that the particles were advected far from the source location. The inverse study portrays the stochastic behavior of the ensemble, which causes some deviation of the location of the maximum probability from the actual release location. The minimum distance between the probability maps and the release location, which indicates the release time of the spill, is detected to be within the release window where the distance was approximately 66.7 km at day 4, the end of the release.

5.2. Continuous release from a moving source

5.2.1. Forward simulation

Release path 3, yellow in Fig. 5, is now considered for the forward moving source experiment. Particles injection starts at Day 3 and ends at Day 4. Snapshots of the probability map are presented for different times in Fig. 9.

The impact of staged injection is observed at Day 4, with the particles released earlier spreading more than later ones, as expected. Here, the particles are released from a location far from the shore and the interaction of the particles with the coast occurs at a later time, with beaching occurring between days 12 and 15 near the North African shore. Prior to Day 12, regions of high probability were concentrated near the release path.

5.2.2. Inverse simulation

Starting with the probability map shown in the top left of Fig. 10 as generated by the forward integration, taken at Day 14, integration of the particles distribution is conducted backward to Day 0. A collection of resulting probability maps at different simulation times of the inverse integration is presented in Fig. 10. The inverse probability map is observed to be advected away from the North African shore. It becomes more diffuse in time due to the stochastic nature of the ensemble, however, the high probability areas of the probability map becomes concentrated near the release path. Beaching occurs at the periphery of the probability map, where particles interact with the Italian coast from as early as Day 9.

5.3. Source identification

The objective function is computed between the inverse probability maps and all seven release paths from Fig. 5 to identify the most

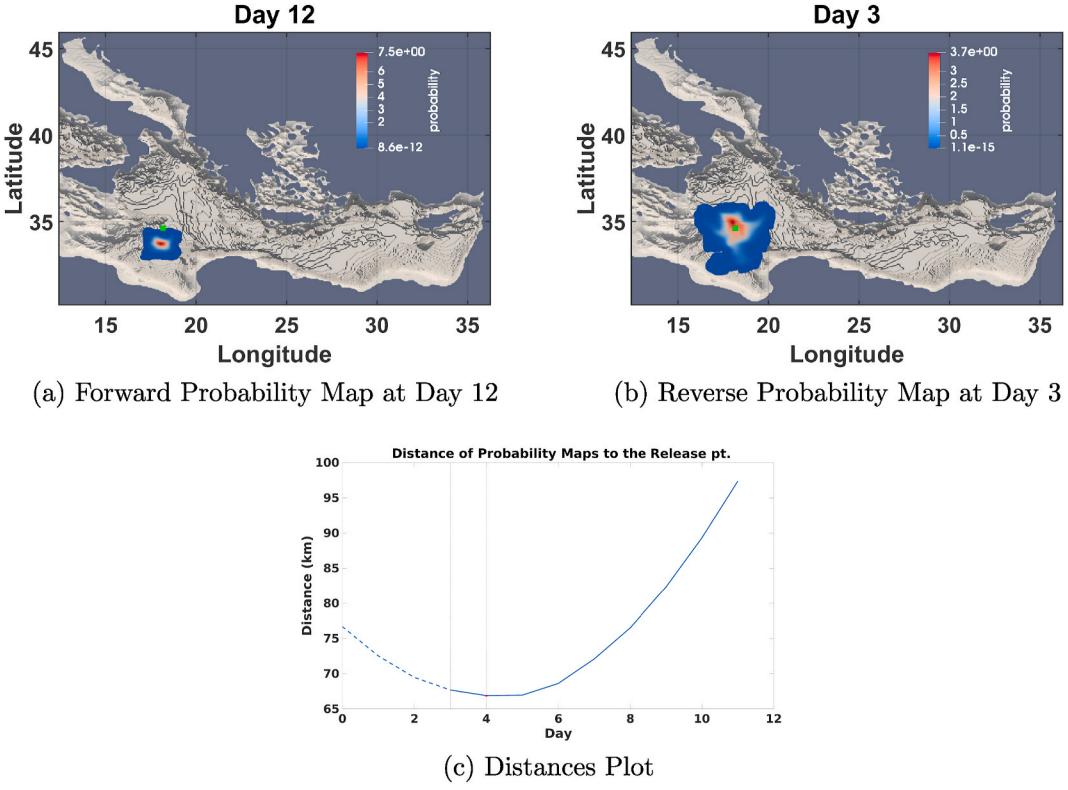

(a) Forward Probability Map at Day 12

(b) Reverse Probability Map at Day 3

(c) Distances Plot

Fig. 8. Probability maps for the continuous release of particles from a fixed source. Shown are: (a) The forward probability map at Day 12 (Observation day), (b) The inverse probability map at Day 3 (actual release day), and (c) The distance plot in time, which shows the release window (dashed vertical lines) and the minimum distance (red dot), dashed blue line shows the distance between the hypothetical distribution (shown because actual release time is unknown). (For interpretation of the references to color in this figure legend, the reader is referred to the Web version of this article.)

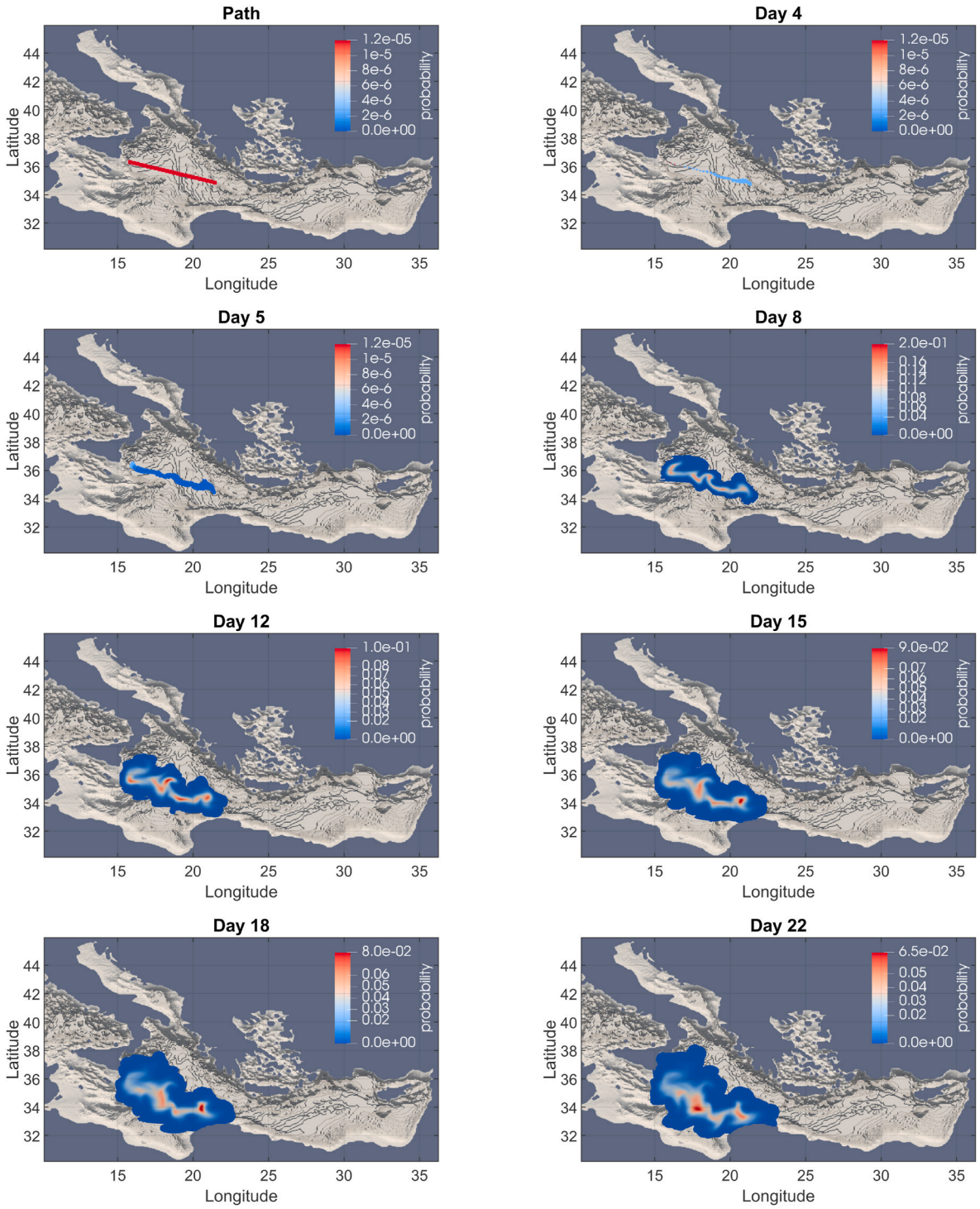

Fig. 9. Instantaneous probabilty maps for a continuous injection from a moving source propagating forward in time. The release segment 3 (top left) is studied with the release beginning at day 3 (top left). A collection of days are chosen as indicated to illustrate the evolution of the particle distribution.

probable polluter among the selected paths. Fig. 11 presents the plots for the resulting objective function with respect to all seven paths along with another plot focusing on the evolution of the objective function relative to path 3, the actual release path in the study.

The results suggest that the most probable release source path is the actual release path, release path 3, which is the closest to all the inverse probability maps. The plot of the objective function computed between the inverse probability maps and release path 3 is convex, with its minimum lying within the release window, where the release time is correctly identified to be Day 4, the end of the release window. This demonstrates that the algorithm is capable of identifying both the release time and path of the pollutant.

5.4. Sensitivity analysis: observation time

This experiment focuses on release path 1 (red in Fig. 5), where the mainstream currents are observed in Fig. 6 to drive particles into the shore, leading to beaching early on. The release path and time are fixed, and different times at which the observation is available are investigated to assess the robustness of the algorithm in identifying the release time

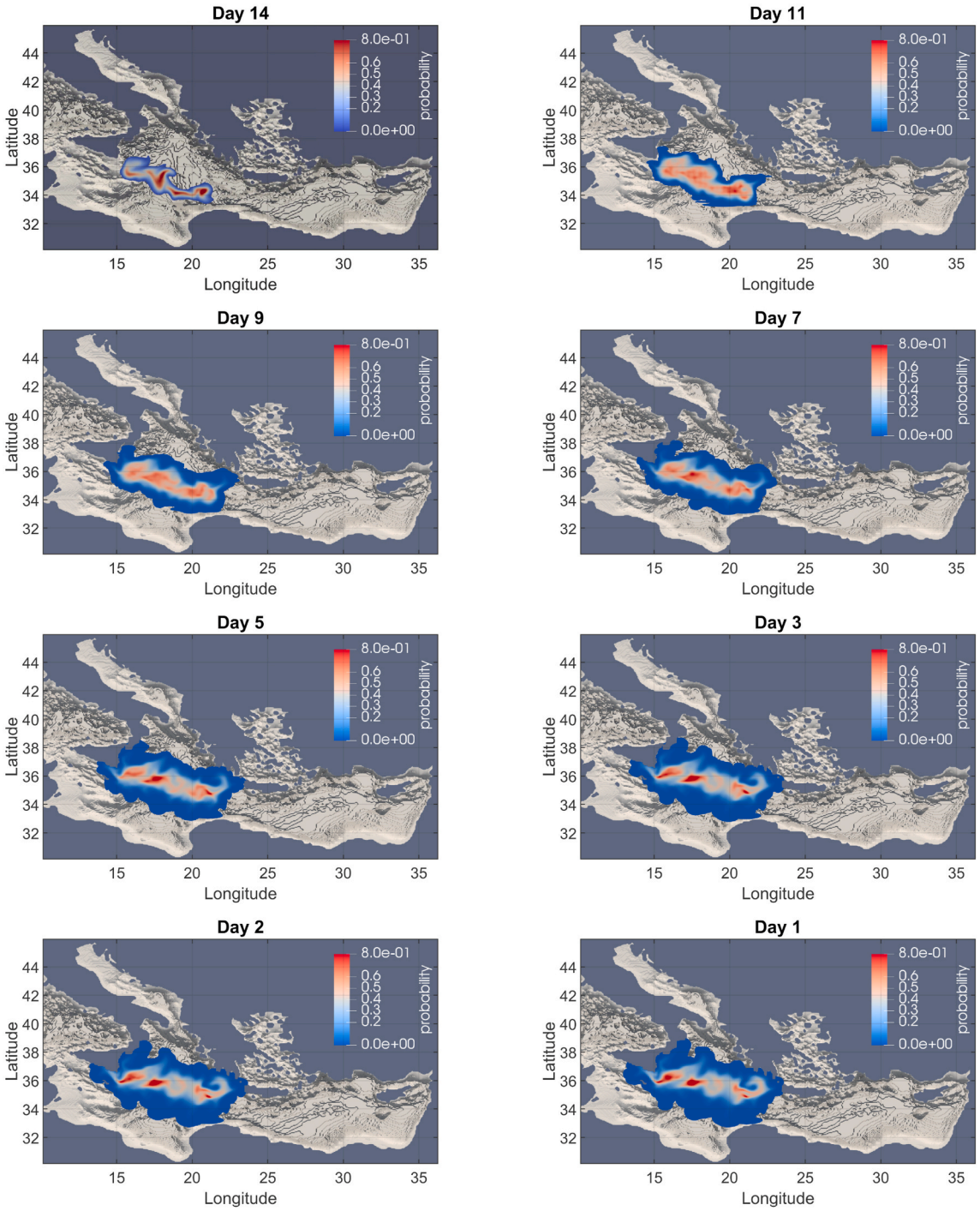

Fig. 10. Probability maps for the inverse simulation case study for the Day 3 release starting from an observation at Day 14 (top left). A collection of days are chosen as indicated to portray the evolution of the probability map going back in time. Note the interaction with the beach at Day 9 near the South of Italy.

and path. In Fig. 12, various curves of the objective function computed with respect to probability maps from different observation times are presented. The closer the observation time is to the release time, the better the algorithm is at pointing to the release window. When beaching effects are dominant, the observation time has to be close to the release time in order to accurately identify the pollutant. Comparing these results to the distances in Fig. 11, we notice that when beaching effects are present, the release time can be identified if the observation is collected at most 5 days after the initial release as opposed to the release from trajectory 3, where the source was identified using an observation collected 12 days after the release.

5.5. *Sensitivity analysis: ensemble variance*

The impact of uncertainties in the ensemble of the flow fields on the identification of the spill time and location is investigated by varying the ensemble variance in the forward and inverse runs. The aim is to examine whether a more certain flow field or a more localized probability map would help better identifying the release source. The sensitivity analysis utilizes a modified ensemble with 50% and 100% of the reference ensemble variance in the forwards simulation, and 100%, 75%, 50%, 25% of the reference ensemble variance along with a deterministic current field that advects particles with the average of the

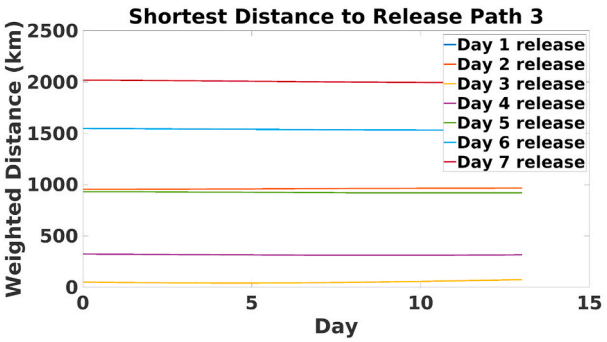

(a) Distance from inverse probability maps to all paths

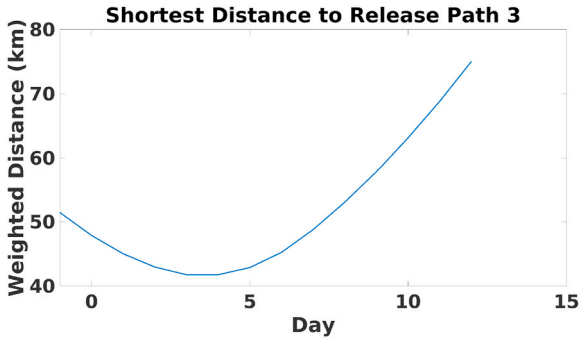

(b) Distance from inverse probability maps to release path 3

Fig. 11. Plot depicting the time evolution of the distances between the probability maps from release 3 to a) all 7 selected paths and b) the release 3 segment.

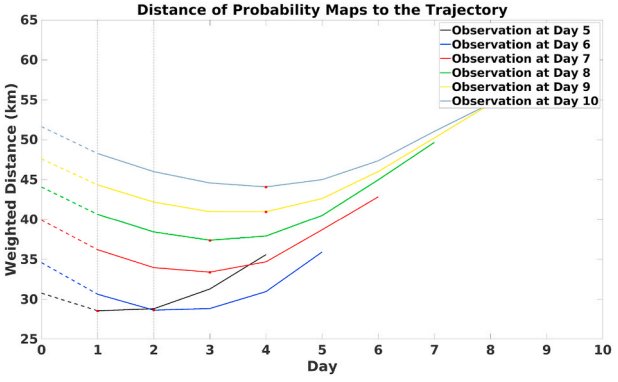

Fig. 12. Plot showing the evolution of the distance between the probability map from release 1 to its path for different observation times. In this study, the percentage of particles beached from day 1 to day 10 were 0%, $8\times\ 10^{-10}$%, 5×10^{-6}%, 5×10^{-4}%, 3×10^{-1}%, 3.3%, 17.6%, 31.2%, $5\times$ 57.5%, 62.1% . Plot shows the release window (dashed vertical lines) and the minimum distance (red dot), dashed blue line shows the distance between the hypothetical distribution (shown because actual release time is unknown). (For interpretation of the references to color in this figure legend, the reader is referred to the Web version of this article.)

ensemble for the inverse study. The ensemble variance is adjusted by spreading its members by a variance fraction, f^2, that represents the fraction of the variance of the new ensemble to the old ensemble. The new ensemble is then generated as:

$$u_i^{(j)}(\vec{x},t) = f^2 u_{i,og}^{(j)}(\vec{x},t) + \left(1-f^2\right)\overline{u_{og}^{(j)}}(\vec{x},t), \tag{6}$$

where, $i = 1,2,\ldots,N_e$ represents the realizations, $j = 1,2,\ldots$ denotes the time index, $u_i^{(j)}(\vec{x},t)$ the i^{th} new ensemble realization of the currents at position $\vec{x}$ and time t, $u_{i,og}^{(j)}$ the i^{th} original ensemble realization and $\overline{u_{og}^{(j)}}$ the average of the original ensemble realizations.

The results, presented in Fig. 13, reveal that a more certain inverse flow field effectively yields a probability map that is closer to the release path than the original ensemble. Snapshots of probability maps at Day 3 are presented in the supplementary to illustrate the effect of the ensemble variance on the spread of the probability maps. The results also suggest that using a more certain flow field in the forward run would yield a tighter probability map, which in turn leads to samples located spatially close to each other, and the objective function was smaller. The accuracy of source identification is noticeably improved when the inverse advection uses a more certain flow field. In particular, the objective function yielded a minimum distance of approximately 93*km* when the particles were advected with an ensemble of flow fields with half the original ensemble variance, as opposed to 115*km* with the original ensemble. Focusing on the case of half ensemble variance in the forward integration, the minimum distance ranged between 86*km*, in the deterministic case, and 104*km*, in the full variance case. To be able to compare with the deterministic case, where the solution is represented by a collection of points instead of a probability map, the objective function was computed based on the average distance.

5.6. Sensitivity analysis: initial number of particles

The sensitivity of the objective function to the initial number of particles from which the inverse study starts is examined by varying the number of sampled particles from the (observed) probability map. The objective function is computed for inverse simulations starting with 1, 10000, 20000, 30000 and 40000 particles, where 40000 particles is the maximum number of particles based on the available computer memory in our case. The number of particles sampled from the observed map corresponds to the observed area, where using less particles may under represent the spill which prevents from accurately identifying the release time.

Fig. 14 presents the distance curves for different initial particles distributions using the objective function. In addition, a sufficiently large collection of particles, which adequately represents the spatial uncertainties, is needed to identify the release time and source. In particular, the more particles are used, the more information is available and the objective function would point to the release time better, which was seen in this experiment where by sampling one particle, the objective function points to Day 0 as the release time whereas using at least $10,000$ particles, the objective function points to the actual release window between Days 3 and 4.

5.7. Investigating more challenging scenarios

Finally, the algorithm is tested on paths that are close to the actual release to further assess its robustness to possible nearby release paths. The selected paths, illustrated in Fig. 15, are as follows:

- The actual path where the release originates.
- Paths that are parallel to the actual release at $\pm 0.5^\circ$ and $\pm 1^\circ$ (paths 1 to 4 respectively).
- A path that is perpendicular to the actual path (path 5).
- Paths that intersect with the actual path with some angle (paths 6 and 7).

The objective function computed between the inverse probability maps and these paths are plotted in Fig. 15, suggesting that the proposed algorithm pinpoints two most likely source ships. This is indicated by the objective functions which yielded comparably close distances to the probability map, 41.2*km* (actual release path) and 41.7*km* (release path 3). In this situation, additional information about the marine traffic may help identify the source ship.

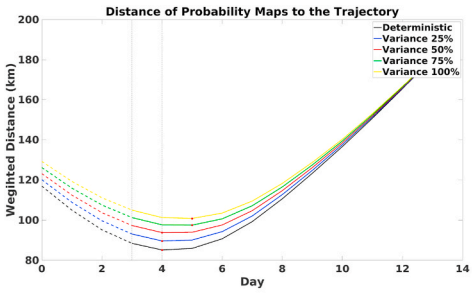

(a) 50% ensemble variance in forwards

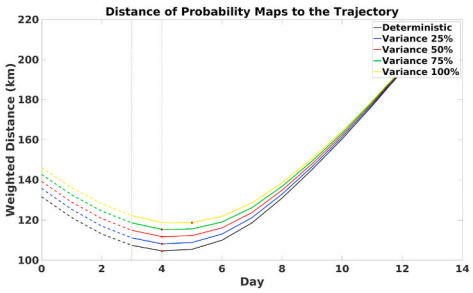

(b) 100% ensemble variance in forwards

Fig. 13. Plot showing the evolution of the distance between the probability map from release 3 to its path for different inverse ensemble variances as indicated in the legend. The distances are computed used normalized aggregate distance in order to have a fair measure with the deterministic study. Plot shows the release window (dashed vertical lines) and the minimum distance (red dot), dashed blue line shows the distance between the hypothetical distribution (shown because actual release time is unknown). (For interpretation of the references to color in this figure legend, the reader is referred to the Web version of this article.)

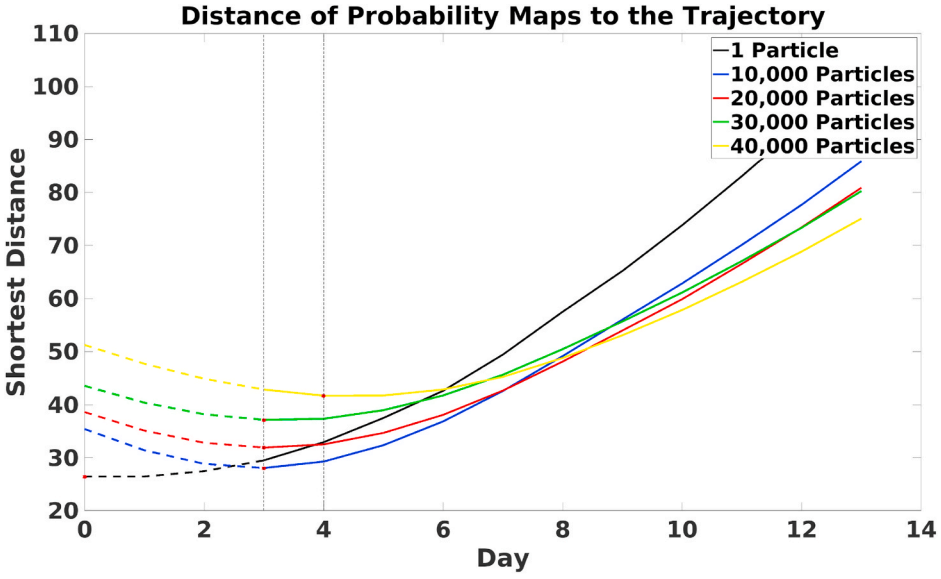

Fig. 14. Plot showing the evolution of the distance between the probability map from release 3 to its path for different initial number of particles for the normalized shortest distance objective function. Plot shows the release window (dashed vertical lines) and the minimum distance (red dot), dashed blue line shows the distance between the hypothetical distribution (shown because actual release time is unknown). (For interpretation of the references to color in this figure legend, the reader is referred to the Web version of this article.)

The results of Fig. 15 show that the path to the south of the actual release has a similar distance to the probability map. This can be explained by the nature of the velocity field in the region, which drives particles northwards in the inverse simulation; therefore, the path 0.5° to the south is expected to have a short distance at a time close to the observation time. Thus, the proposed methodology provides a systematic approach to rule out ship paths that do not belong to probable polluters.

6. Conclusion

We proposed a new methodology for identifying the release time and path of pollutants from fixed and moving sources. The proposed methodology relies on an LPT algorithm capable of backward integration and accommodates deterministic and stochastic flow fields. A staged particle injection algorithm for the forward particle tracking from fixed and moving sources was implemented. Backward particle tracking starting from an observed map, which could be deterministic or probabilistic, was introduced along with proper filtering of particles trapped at the coast or particles of low probability. The identification of the release time and trajectory was formulated as determining the minimum of an objective function measuring the distance between inverse probability maps and release trajectories, weighted by the probability of the particle to be at its corresponding location.

Source identification was tested with our LPT operating with an uncertain flow in the Mediterranean Sea. The results of the numerical experiments suggest that the proposed methodology could successfully identify the release time and location for up to two weeks when the effects of coastal interactions are weak, and up to 5 days when particles interact heavily with the coast. The results also suggest that the proposed methodology could also be used to shortlist the probable polluters in challenging scenarios, where densely operated paths are nearby or intersecting.

In future work, we shall augment our LPT with a physical model to simulate specific pollution spills such as oil spills. This may require developing a more sophisticated inversion such as Bayesian inference to address the nonlinear irreversible nature of the pollution dynamics and weathering effects. A Bayesian inference framework, however, will be computationally prohibitive in a realistic setting as the sampling of the posterior distribution of the parameters of interest will require evaluating the likelihood using the pollution model for each sample of the parameters to be inverted. We will explore surrogate models to alleviate the computational burden of such an approach. We also plan to investigate other more sophisticated beaching models to mitigate the loss of information caused by coastal interactions.

CRediT authorship contribution statement

Mohamad Abed El Rahman Hammoud: Methodology, Visualization, Investigation, Software, Writing - original draft. **Issam Lakkis:**

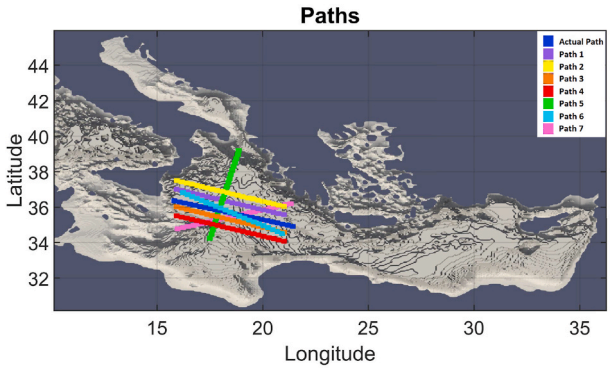

(a) Paths Studied

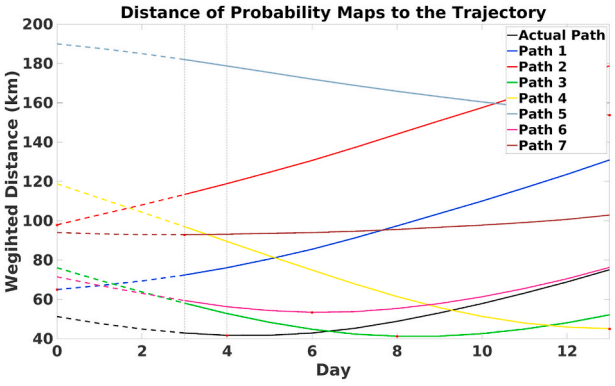

(b) Distances Plot

Fig. 15. Plot showing the evolution of distance from the probability map of release 3 to the paths studied shown in (a), the plot in (b) compares the trends for these different paths. Plot shows the release window (dashed vertical lines) and the minimum distance (red dot), dashed blue line shows the distance between the hypothetical distribution (shown because actual release time is unknown). (For interpretation of the references to color in this figure legend, the reader is referred to the Web version of this article.)

Conceptualization, Supervision, Software, Writing - review & editing. **Omar Knio:** Conceptualization, Methodology, Supervision, Writing - review & editing, Funding acquisition. **Ibrahim Hoteit:** Conceptualization, Methodology, Supervision, Writing - review & editing, Funding acquisition.

Declaration of competing interest

The authors declare that they have no known competing financial interests or personal relationships that could have appeared to influence the work reported in this paper.

Acknowledgments

Research reported in this publication was supported by the Office of Sponsored Research (OSR) at King Abdullah University of Science and Technology (KAUST) CRG Award No. OSR-CRG2018-3711 and Virtual Red Sea Initiative (Grant #REP/1/3268-01-01) and by the University Research Board of the American University of Beirut (AUB). We acknowledge the use of E.U. Copernicus Marine Service Information available at https://doi.org/10.25423/MEDSEA_REANALYSIS_PHYS_006_004.

Appendix A. Supplementary data

Supplementary data to this article can be found online at https://doi.org/10.1016/j.oceaneng.2020.108435.

References

Annika, P., George, T., George, P., Konstantinos, N., Costas, D., Koutitas, C., 2001. The poseidon operational tool for the prediction of floating pollutant transport. Mar. Pollut. Bull. 43, 270–278. https://doi.org/10.1016/S0025-326X(01)00080-7. http://www.sciencedirect.com/science/article/pii/S0025326X01000807. marine Environmental Modelling.

Batchelder, H.P., 2006. Forward-in-time-/backward-in-time-trajectory (fitt/bitt) modeling of particles and organisms in the coastal ocean. J. Atmos. Ocean. Technol. 23, 727–741. https://doi.org/10.1175/JTECH1874.1.

Beaudoin, A., de Dreuzy, J.R., Erhel, J., 2007. An efficient parallel particle tracker for advection-diffusion simulations in heterogeneous porous media. In: Kermarrec, A. M., Bougé, L., Priol, T. (Eds.), Euro-Par 2007 Parallel Processing. Springer Berlin Heidelberg, Berlin, Heidelberg, pp. 717–726.

Bennett, K.E., Werner, A.T., Schnorbus, M., 2012. Uncertainties in hydrologic and climate change impact analyses in headwater basins of british columbia. J. Clim. 25, 5711–5730. https://doi.org/10.1175/JCLI-D-11-00417.1.

Breivik, Ø., Bekkvik, T.C., Wettre, C., Ommundsen, A., 2011. BAKTRAK: backtracking drifting objects using an iterative algorithm with a forward trajectory model. Ocean Dynam. 62, 239–252. https://doi.org/10.1007/s10236-011-0496-2 doi:10.1007/s10236-011-0496-2.

Brickman, D., Smith, P.C., 2002. Lagrangian stochastic modeling in coastal oceanography. J. Atmos. Ocean. Technol. 19, 83–99. https://doi.org/10.1175/1520-0426(2002)019<0083:LSMICO>2.0.CO;2.

Coppini, G., Dominicis, M.D., Zodiatis, G., Lardner, R., Pinardi, N., Santoleri, R., Colella, S., Bignami, F., Hayes, D.R., Soloviev, D., Georgiou, G., Kallos, G., 2011. Hindcast of oil-spill pollution during the Lebanon crisis in the eastern mediterranean, july–august 2006. Mar. Pollut. Bull. 62, 140–153. https://doi.org/10.1016/j.marpolbul.2010.08.021 doi:10.1016/j.marpolbul.2010.08.021.

De Dominicis, M., Pinardi, N., Zodiatis, G., Archetti, R., 2013a. MEDSLIK-II, a Lagrangian marine surface oil spill model for short-term forecasting-Part 2: numerical simulations and validations. Geosci. Model Dev. (GMD) 6, 1871–1888. https://doi.org/10.5194/gmd-6-1871-2013.

De Dominicis, M., Pinardi, N., Zodiatis, G., Lardner, R., 2013b. MEDSLIK-II, a Lagrangian marine surface oil spill model for short-term forecasting-Part 1: Theory. Geosci. Model Dev. (GMD) 6, 1851–1869. https://doi.org/10.5194/gmd-6-1851-2013.

Duncan, E.M., Arrowsmith, J., Bain, C., Broderick, A.C., Lee, J., Metcalfe, K., Pikesley, S. K., Snape, R.T., van Sebille, E., Godley, B.J., 2018. The true depth of the mediterranean plastic problem: extreme microplastic pollution on marine turtle nesting beaches in Cyprus. Mar. Pollut. Bull. 136, 334–340. https://doi.org/10.1016/j.marpolbul.2018.09.019. http://www.sciencedirect.com/science/article/pii/S0025326X18306581.

Edwards, C.A., Moore, A.M., Hoteit, I., Cornuelle, B.D., 2015. Regional ocean data assimilation. Annual Review of Marine Science 7, 21–42. https://doi.org/10.1146/annurev-marine-010814-015821.

El-Mohtar, S., Hoteit, I., Knio, O., Issa, L., Lakkis, I., 2018. Lagrangian tracking in stochastic fields with application to an ensemble of velocity fields in the red sea. Ocean Model. 131, 1–14. https://doi.org/10.1016/j.ocemod.2018.08.008. http://www.sciencedirect.com/science/article/pii/S1463500318300490.

Girin, M., Carpenter, A., 2018. Shipping and oil transportation in the mediterranean sea. In: Carpenter, A., Kostianoy, A.G. (Eds.), Oil Pollution in the Mediterranean Sea: Part I: the International Context. Springer International Publishing, Cham, pp. 33–51. https://doi.org/10.1007/698_2017_6 doi:10.1007/698_2017_6.

Golub, G.H., Reinsch, C., 1971. Singular value decomposition and least squares solutions. In: Linear Algebra. Springer, pp. 134–151.

Groves, D.G., Yates, D., Tebaldi, C., 2008. Developing and applying uncertain global climate change projections for regional water management planning. Water Resour. Res. 44 https://doi.org/10.1029/2008WR006964 arXiv:https://agupubs.onlinelibrary.wiley.com/doi/pdf/10.1029/2008WR006964. https://agupubs.onlinelibrary.wiley.com/doi/abs/10.1029/2008WR006964.

Guo, H., He, W., Seo, S., Shen, H., Constantinescu, E.M., Liu, C., Peterka, T., 2019. Extreme-scale stochastic particle tracing for uncertain unsteady flow visualization and analysis. IEEE Trans. Visual. Comput. Graph. 25, 2710–2724. https://doi.org/10.1109/TVCG.2018.2856772.

Guo, H., Yuan, X., Huang, J., Zhu, X., 2013. Coupled ensemble flow line advection and analysis. IEEE Trans. Visual. Comput. Graph. 19, 2733–2742. https://doi.org/10.1109/TVCG.2013.144.

Havens, H., Luther, M.E., Meyers, S.D., Heil, C.A., 2010. Lagrangian particle tracking of a toxic dinoflagellate bloom within the tampa bay estuary. Mar. Pollut. Bull. 60, 2233–2241. https://doi.org/10.1016/j.marpolbul.2010.08.013. http://www.sciencedirect.com/science/article/pii/S0025326X10003899.

Hollt, T., Hadwiger, M., Knio, O., Hoteit, I., 2015. Probability maps for the visualization of assimilation ensemble flow data. In: Middel, A., Rink, K., Weber, G.H. (Eds.), Workshop on Visualisation in Environmental Sciences (EnvirVis), the Eurographics Association. https://doi.org/10.2312/envirvis.20151090.

Hoteit, I., Cornuelle, B., Heimbach, P., 2010. An eddy-permitting, dynamically consistent adjoint-based assimilation system for the tropical pacific: hindcast experiments in 2000. J. Geophys. Res. 115 https://doi.org/10.1029/2009jc005437 doi:10.1029/2009jc005437.

Hoteit, I., Hoar, T., Gopalakrishnan, G., Collins, N., Anderson, J., Cornuelle, B., Köhl, A., Heimbach, P., 2013. A mitgcm/dart ensemble analysis and prediction system with application to the gulf of Mexico. Dynam. Atmos. Oceans 63, 1–23. https://doi.org/10.1016/j.dynatmoce.2013.03.002. http://www.sciencedirect.com/science/article/pii/S0377026513000249.

Hoteit, I., Luo, X., Bocquet, M., Köhl, A., Ait-El-Fquih, B., 2018. Data assimilation in oceanography: current status and new directions. In: New Frontiers in Operational

Oceanography. GODAE OceanView. https://doi.org/10.17125/gov2018.ch17 doi:10.17125/gov2018.ch17.
Hoteit, I., Pham, D.T., Blum, J., 2001. A semi-evolutive partially local filter for data assimilation. Mar. Pollut. Bull. 43, 164–174. https://doi.org/10.1016/S0025-326X(01)00079-0 marine Environmental Modelling. http://www.sciencedirect.com/science/article/pii/S0025326X01000790.
Ivorra, B., Gomez, S., Glowinski, R., Ramos, A.M., 2016. Nonlinear advection–diffusion–reaction phenomena involved in the evolution and pumping of oil in open sea: modeling, numerical simulation and validation considering the prestige and oleg naydenov oil spill cases. J. Sci. Comput. 70, 1078–1104. https://doi.org/10.1007/s10915-016-0274-x doi:10.1007/s10915-016-0274-x.
Kao, T.Y., Elsayed, E., 1990. Performance of the lpt algorithm in multiprocessor scheduling. Comput. Oper. Res. 17, 365–373. https://doi.org/10.1016/0305-0548(90)90015-Y. http://www.sciencedirect.com/science/article/pii/030505489090015Y.
Kostianoy, A.G., Carpenter, A., 2018a. History, sources and volumes of oil pollution in the mediterranean sea. In: Carpenter, A., Kostianoy, A.G. (Eds.), Oil Pollution in the Mediterranean Sea: Part I: the International Context. Springer International Publishing, Cham, pp. 9–31. https://doi.org/10.1007/698_2018_369 doi:10.1007/698_2018_369.
Kostianoy, A.G., Carpenter, A., 2018b. Oil and gas exploration and production in the mediterranean sea. In: Carpenter, A., Kostianoy, A.G. (Eds.), Oil Pollution in the Mediterranean Sea: Part I: the International Context. Springer International Publishing, Cham, pp. 53–77. https://doi.org/10.1007/698_2018_373 doi:10.1007/698_2018_373.
Lardner, R., Zodiatis, G., 2016. MEDSLIK oil spill model recent developments. In: EGU General Assembly Conference Abstracts, pp. EPSC2016–16240.
Lardner, R., Zodiatis, G., 2017. Modelling oil plumes from subsurface spills. Mar. Pollut. Bull. 124, 94–101. https://doi.org/10.1016/j.marpolbul.2017.07.018 doi:10.1016/j.marpolbul.2017.07.018.
Lett, C., Verley, P., Mullon, C., Parada, C., Brochier, T., Penven, P., Blanke, B., 2008. A Lagrangian tool for modelling ichthyoplankton dynamics. Environ. Model. Software 23, 1210–1214. https://doi.org/10.1016/j.envsoft.2008.02.005.
Liu, Y., Weisberg, R.H., Hu, C., Zheng, L., 2013. Trajectory forecast as a rapid response to the deepwater Horizon oil spill. Monitoring and modeling the deepwater Horizon. Oil Spill: A Record Breaking Enterprise 153–165. https://doi.org/10.1029/2011GM001121.
Liubartseva, S., Coppini, G., Lecci, R., Clementi, E., 2018. Tracking plastics in the mediterranean: 2d Lagrangian model. Mar. Pollut. Bull. 129, 151–162. https://doi.org/10.1016/j.marpolbul.2018.02.019 doi:10.1016/j.marpolbul.2018.02.019.
Liubartseva, S., Coppini, G., Lecci, R., Creti, S., 2016. Regional approach to modeling the transport of floating plastic debris in the adriatic sea. Mar. Pollut. Bull. 103, 115–127. https://doi.org/10.1016/j.marpolbul.2015.12.031 doi:10.1016/j.marpolbul.2015.12.031.
Niu, H., Li, Z., Lee, K., Kepkay, P., Mullin, J., 2010. A method for assessing environmental risks of oil-mineral-aggregate to benthic organisms. Hum. Ecol. Risk Assess. 16, 762–782. https://doi.org/10.1080/10807039.2010.501240.
North, E.W., Adams, E.E., Schlag, Z., Sherwood, C.R., He, R., Hyun, K.H., Socolofsky, S.A., 2013. Simulating oil droplet dispersal from the deepwater Horizon spill with a Lagrangian approach. Monitoring and Modeling the Deepwater Horizon Oil Spill: A Record Breaking Enterprise 217–226. https://doi.org/10.1029/2011GM001102.
Otote, A.D., Li, B., Ai, B., Gao, S., Xu, J., Chen, X., Lv, G., 2019. A decision-making algorithm for maritime search and rescue plan. Sustainability 11. https://doi.org/10.3390/su11072084. https://www.mdpi.com/2071-1050/11/7/2084.
Perivoliotis, L., Krokos, G., Nittis, K., Korres, G., 2011. The aegean sea marine security decision support system. Ocean Sci. 7, 671–683. https://doi.org/10.5194/os-7-671-2011. https://www.ocean-sci.net/7/671/2011/.
Petihakis, G., Triantafyllou, G., Allen, I.J., Hoteit, I., Dounas, C., 2002. Modelling the spatial and temporal variability of the cretan sea ecosystem. J. Mar. Syst. 36, 173–196. https://doi.org/10.1016/S0924-7963(02)00186-0. http://www.sciencedirect.com/science/article/pii/S0924796302001860.
Pourmehran, O., Rahimi-Gorji, M., Gorji-Bandpy, M., Gorji, T.B., 2015. Simulation of magnetic drug targeting through tracheobronchial airways in the presence of an external non-uniform magnetic field using Lagrangian magnetic particle tracking. J. Magn. Magn Mater. 393, 380–393. https://doi.org/10.1016/j.jmmm.2015.05.086 doi:10.1016/j.jmmm.2015.05.086.
Preisendorfer, R.W., Mobley, C.D., 1988. Principal component analysis in meteorology and oceanography. Dev. Atmos. Sci. 17.
Raitsos, D.E., Brewin, R.J.W., Zhan, P., Dreano, D., Pradhan, Y., Nanninga, G.B., Hoteit, I., 2017. Sensing coral reef connectivity pathways from space. Sci. Rep. 7 https://doi.org/10.1038/s41598-017-08729-w doi:10.1038/s41598-017-08729-w.
Schuster, B.S., Ensign, L.M., Allan, D.B., Suk, J.S., Hanes, J., 2015. Particle tracking in drug and gene delivery research: state-of-the-art applications and methods. Adv. Drug Deliv. Rev. 91, 70–91. https://doi.org/10.1016/j.addr.2015.03.017 doi:10.1016/j.addr.2015.03.017.
van Sebille, E., Griffies, S.M., Abernathey, R., Adams, T.P., Berloff, P., Biastoch, A., Blanke, B., Chassignet, E.P., Cheng, Y., Cotter, C.J., Deleersnijder, E., Döös, K., Drake, H.F., Drijfhout, S., Gary, S.F., Heemink, A.W., Kjellsson, J., Koszalka, I.M., Lange, M., Lique, C., MacGilchrist, G.A., Marsh, R., Mayorga Adame, C.G., McAdam, R., Nencioli, F., Paris, C.B., Piggott, M.D., Polton, J.A., Rühs, S., Shah, S.H., Thomas, M.D., Wang, J., Wolfram, P.J., Zanna, L., Zika, J.D., 2018. Lagrangian ocean analysis: fundamentals and practices. Ocean Model. 121, 49–75. https://doi.org/10.1016/j.ocemod.2017.11.008.
van Sebille, E., Wilcox, C., Lebreton, L., Maximenko, N., Hardesty, B.D., van Franeker, J.A., Eriksen, M., Siegel, D., Galgani, F., Law, K.L., 2015. A global inventory of small floating plastic debris. Environ. Res. Lett. 10, 124006. https://doi.org/10.1088/1748-9326/10/12/124006.
Sentchev, A., Korotenko, K., 2007. Modelling distribution of flounder larvae in the eastern English Channel: sensitivity to physical forcing and biological behaviour. Mar. Ecol. Prog. Ser. 347, 233–245. https://doi.org/10.3354/meps06981.
Wang, G., Oyana, T., Zhang, M., Adu-Prah, S., Zeng, S., Lin, H., Se, J., 2009. Mapping and spatial uncertainty analysis of forest vegetation carbon by combining national forest inventory data and satellite images. For. Ecol. Manag. 258, 1275–1283. https://doi.org/10.1016/j.foreco.2009.06.056. http://www.sciencedirect.com/science/article/pii/S0378112709004253.
Wang, Y., Raitsos, D.E., Krokos, G., Gittings, J.A., Zhan, P., Hoteit, I., 2019. Physical connectivity simulations reveal dynamic linkages between coral reefs in the southern red sea and the indian ocean. Sci. Rep. 9 https://doi.org/10.1038/s41598-019-53126-0 doi:10.1038/s41598-019-53126-0.
Wichmann, D., Delandmeter, P., Sebille, E., 2019. Influence of near-surface currents on the global dispersal of marine microplastic. J. Geophys. Res.: Oceans. https://doi.org/10.1029/2019jc015328.
Yee, E., 2007. Bayesian probabilistic approach for inverse source determination from limited and noisy chemical or biological sensor concentration measurements. In: Fountain III, A.W. (Ed.), Chemical and Biological Sensing VIII. International Society for Optics and Photonics, SPIE, pp. 255–266. https://doi.org/10.1117/12.721630.
Zhang, Q., Zhang, P., 2019. An uncertainty descriptor for quantitative measurement of the uncertainty of remote sensing images. Rem. Sens. 11 https://doi.org/10.3390/rs11131560. https://www.mdpi.com/2072-4292/11/13/1560.
Zhao, B., Chen, C., Lai, A.C.K., 2011. Lagrangian stochastic particle tracking: further discussion. Aerosol. Sci. Technol. 45, 901–902. https://doi.org/10.1080/02786826.2011.570382.
Zodiatis, G., Coppini, G., Perivoliotis, L., Lardner, R., Alves, T., Pinardi, N., Liubartseva, S., Dominicis, M.D., Bourma, E., Neves, A.A.S., 2017. Numerical modeling of oil pollution in the eastern mediterranean sea. In: The Handbook of Environmental Chemistry. Springer International Publishing, pp. 215–254. https://doi.org/10.1007/698_2017_131 doi:10.1007/698_2017_131.
Zodiatis, G., Lardner, R., Solovyov, D., Panayidou, X., Dominicis, M.D., 2012. Predictions for oil slicks detected from satellite images using myocean forecasting data. http://hdl.handle.net/2122/8643.